*Mon. Not. R. astr. Soc.* (1970) **151**, 109–122.

# DISTRIBUTION OF BRIGHTNESS AND POLARIZATION IN CASSIOPEIA A AT 5·0 GHz

*Ivan Rosenberg*

(Communicated by P. A. G. Scheuer)

(Received 1970 July 6)

SUMMARY

Cas A (3C 461) has been observed at a frequency of 5·0 GHz with a resolving power of $6''\cdot5 \times 7''\cdot6$ arc. Further resolution of the fine structure is revealed in the distribution of total intensity, and a study of the variations of structure with frequency is presented. Linear polarization of about 5 per cent has been found around the rim of the source, consistent with a radial component of magnetic field. The distribution of total emission from the source is shown to be consistent with this configuration of magnetic field.

## 1. INTRODUCTION

In a previous paper (Rosenberg 1970, henceforth referred to as Paper I) a radio map was presented of the supernova remnant Cas A (3C 461), made with the Cambridge One-Mile telescope (Ryle 1962) at a frequency of 2·7 GHz and a resolving power of $12'' \times 14''$ arc. While Paper I was in press, a map was published by Hogg *et al.* (1969) also at 2·7 GHz and with a somewhat higher resolving power. Although the majority of the large scale structure was not observable with their instrument, the finer scale features on the maps agree well.

Further details of the source are now available from observations of the intensity and polarization distributions at 5·0 GHz with a resolving power of $6''\cdot5 \times 7''\cdot6$ arc and some of the conclusions reached in Paper I require modification in the light of these new data.

The observations are described in Section 2 and the distribution of total emission in Section 3. Changes of structure with frequency are considered in Section 4 and the distribution of polarized emission is presented in Section 5. The physical characteristics of the source are discussed briefly in Section 6.

## 2. OBSERVATIONS

The source was observed during the period 1969 October–November, using the Cambridge One-Mile telescope (Elsmore, Kenderdine & Ryle 1966) operating at a frequency of 4·995 GHz. The telescope synthesizes an aperture consisting of equally spaced concentric annuli lying in the equatorial plane. To ensure that the first grating response did not affect the observations, the annuli were separated by $390\lambda$; this required 64 spacings of the interferometer. The data thus collected were processed to give a synthesized reception pattern of width $6''\cdot5$ arc in R.A. and $7''\cdot6$ arc in declination between the half-power points and a first sidelobe response of 5 per cent.

By a time-sharing procedure, the brightness distribution was observed in three linear polarizations, with electric vectors in position angles 0°, 45° and 90°. The linearly polarized feeds of the three aerials were kept parallel to each other throughout the observations, but were rotated to the above angles for successive two-minute periods. The collimation error of the telescope was calibrated by means of the source 3C 286, unresolved at the maximum baseline used; the sensitivity scale was based on an adopted flux of $8 \cdot 18 \times 10^{-26}$ W m$^{-2}$ Hz$^{-1}$ for the source 3C 147 (Kellermann, Pauliny-Toth & Williams 1969). The sensitivities of the three feed orientations were investigated by observing 3C 84 and 3C 147 for 12 hours each at one spacing. The degrees of polarization of these two sources are known to be less than 1 per cent (Sastry, Pauliny-Toth & Kellerman 1967) and were taken to be zero. The relative amplitudes measured for both 3C 84 and 3C 147 were

1·01 in p.a. 0°
1·00 in p.a. 45°
0·99 in p.a. 90°.

The amplitudes observed for Cassiopeia A were therefore normalized by dividing by the above factors. Systematic errors in phase, which result in a shift of the apparent position of the source, were also determined from observations of 3C 84. Thus, a constant 5° difference between the phase determined at p.a. 0° and at p.a. 90° was found and removed from the Cassiopeia A phase measurements. The primary reception pattern of each dish is circularly symmetrical to within 2 per cent out to 5′ arc from the centre of the beam; therefore, corrections for changes in primary pattern with feed orientation were not necessary. A further source of error arises if the three maps have different zero levels; prior to subtraction the zero levels were determined by averaging over regions well away from the source and they were found to be identical. The corrections to the data from the above known effects leave an uncertainty of about 1 per cent for the instrumental polarization.

So long as the relative position of the aerials due to the Earth's rotation changes by less than $390\lambda$ during one cycle of this procedure (8 min, including the time for the actual rotation of the feeds), the sampling interval is still determined by the separation between successive annuli and no additional grating responses will affect maps synthesized using only observations made at one particular feed orientation.

The above condition was not fulfilled for the largest spacings used; the total intensity map (Section 3) was, however, synthesized using all the observations as if no feed rotation had occurred. It is, therefore, a mean of all three polarization distributions; since the polarization is small (Section 5), this is virtually the same as the true distribution of total emission. The polarized intensity distribution obtained by synthesizing three maps with different feed orientations was, on the other hand, convolved to an effective resolution of 23″ × 27″ arc (Section 5) in order to improve the signal-to-noise ratio; for the spacings which contribute to this convolved distribution the above condition was satisfied.

## 3. DISTRIBUTION OF TOTAL EMISSION

The distribution of total emission from Cas A at 5·0 GHz is shown in Fig. 1 as profiles across the source at intervals of 3″·2 arc in declination. A map of con-

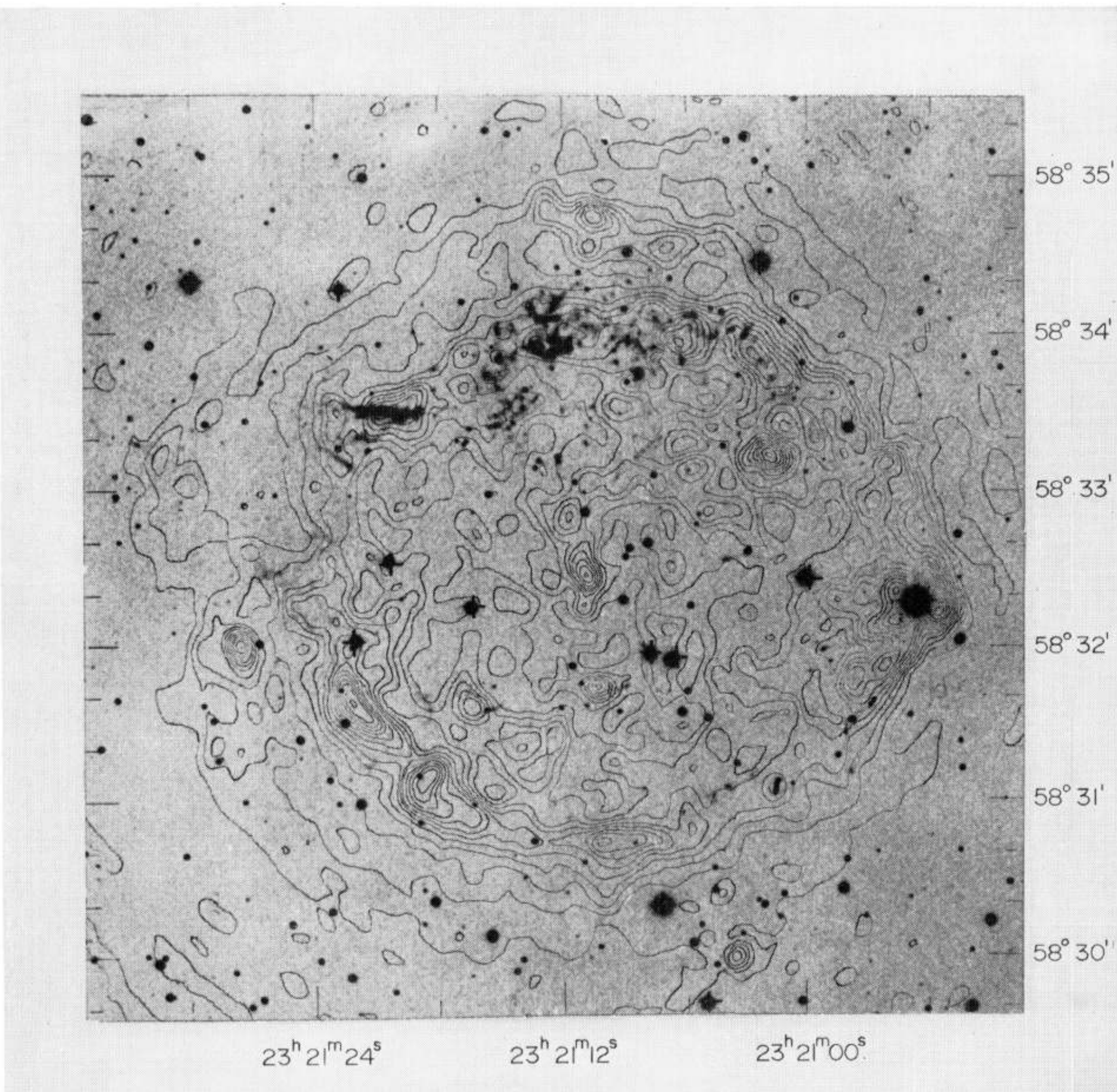




PLATE I. *Mt Wilson and Palomar Observatory photograph of Cas A, courtesy of S. van den Bergh. The 5·0 GHz map is superimposed.*

[*facing p.* 110]

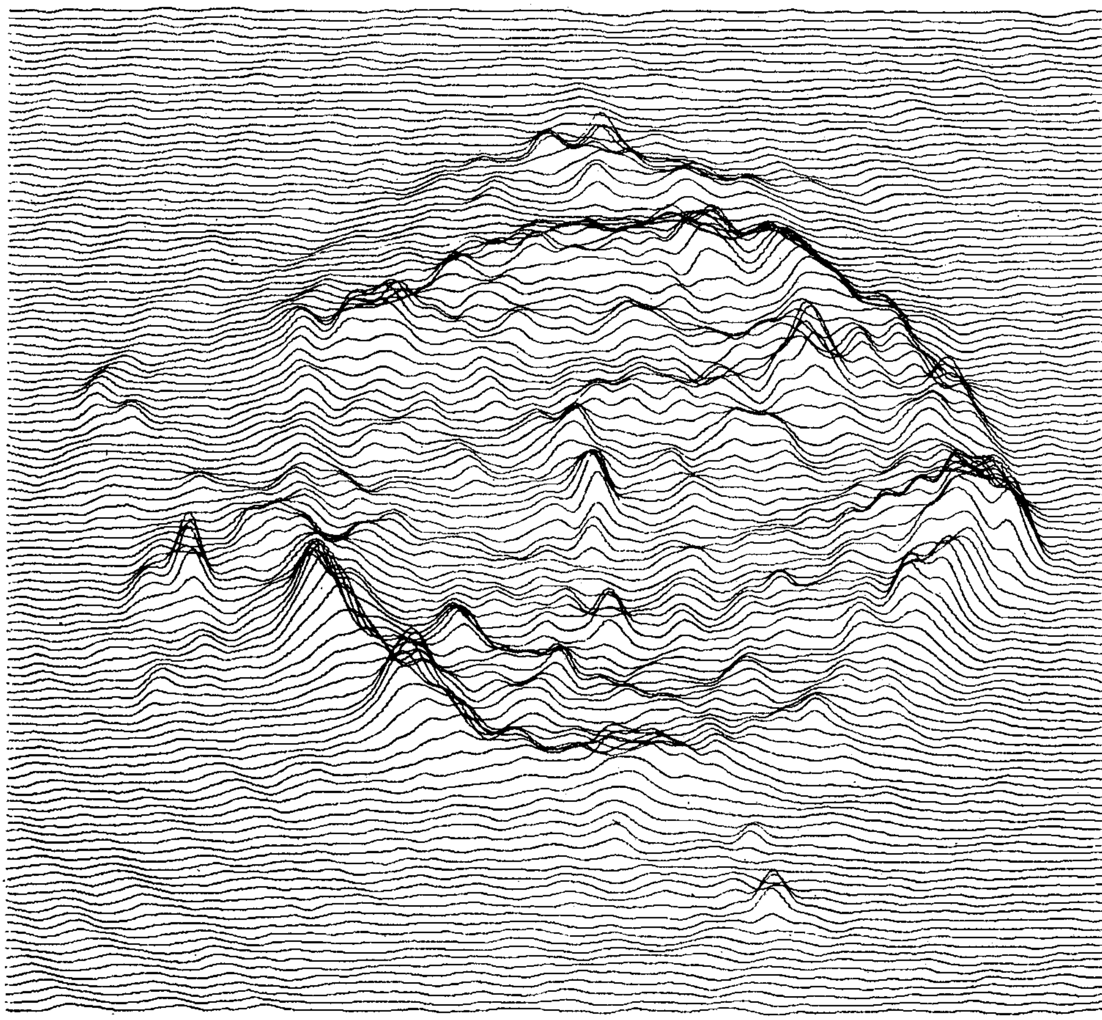

FIG. 1. *Profiles across Cas A at 4·995 GHz. The declination interval is 3″·2 arc.*

tours of equal brightness temperature in the sky (at intervals of 200 °K) is shown in Fig. 2 and also on Plate I, superimposed on a recent photograph of the optical filaments (van den Bergh, private communication). The positions of the radio features are believed to be accurate to better than 2″ arc. The positions of the optical features are based on new measurements of star positions in the field by Murray (private communication) the accuracy of which is better than 0″·2 arc. It can be seen from Plate I that the northern arc of nebulosities is wholly contained within the radio shell, and so are most of the scattered semi-stationary filaments in the southern part of the source but, in general, there is no detailed correspondence between the fine radio structure and the optical filaments.

The main radio features discussed in Paper I can be easily recognized in Fig. 2. The peaks of stronger emission are more clearly separated with the higher resolving power of the new map, and a large number of features which were weak and not obviously significant on the 2·7 GHz map are clearly confirmed.

A total of 80 local maxima of intensity can be identified, most of them arising from further resolution of the 25 peaks of enhanced emission discussed in Paper I.

All the peaks are partially resolved and it is clear that with still higher resolving power they would be split again into still smaller structure. The distribution over the source and some physical characteristics of these regions are discussed in Section 6.

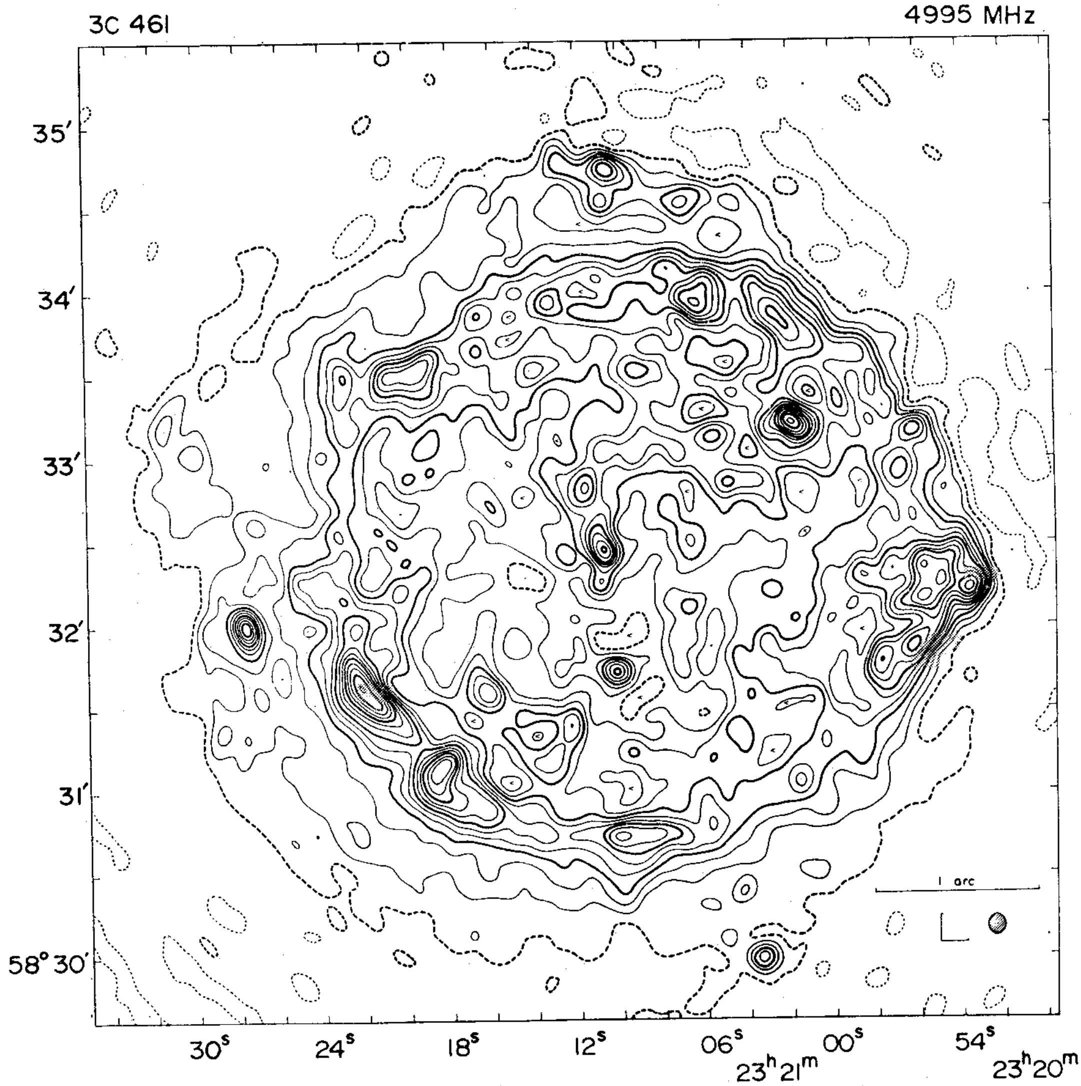


FIG. 2. *Contours of Cas A at* 4·995 *GHz. Coordinates are for epoch* 1950·0. *The contour interval is* 200 °*K. The thick dashed contour represents the zero contour. The half-power beamwidth of the radio telescope* (6″·5 × 7″·6 *arc*) *is also shown. Isolated minima are indicated by the symbol* $<$.

The plateau of weaker emission surrounding most of the shell is even more evident on the 5·0 GHz than on the 2·7 GHz map. The apparent further extension to the north on the 2·7 GHz map was caused by a computational error which displaced the large-scale components of the observed emission (corresponding to the smallest spacing between the aerials) by about 1′ arc north of the true

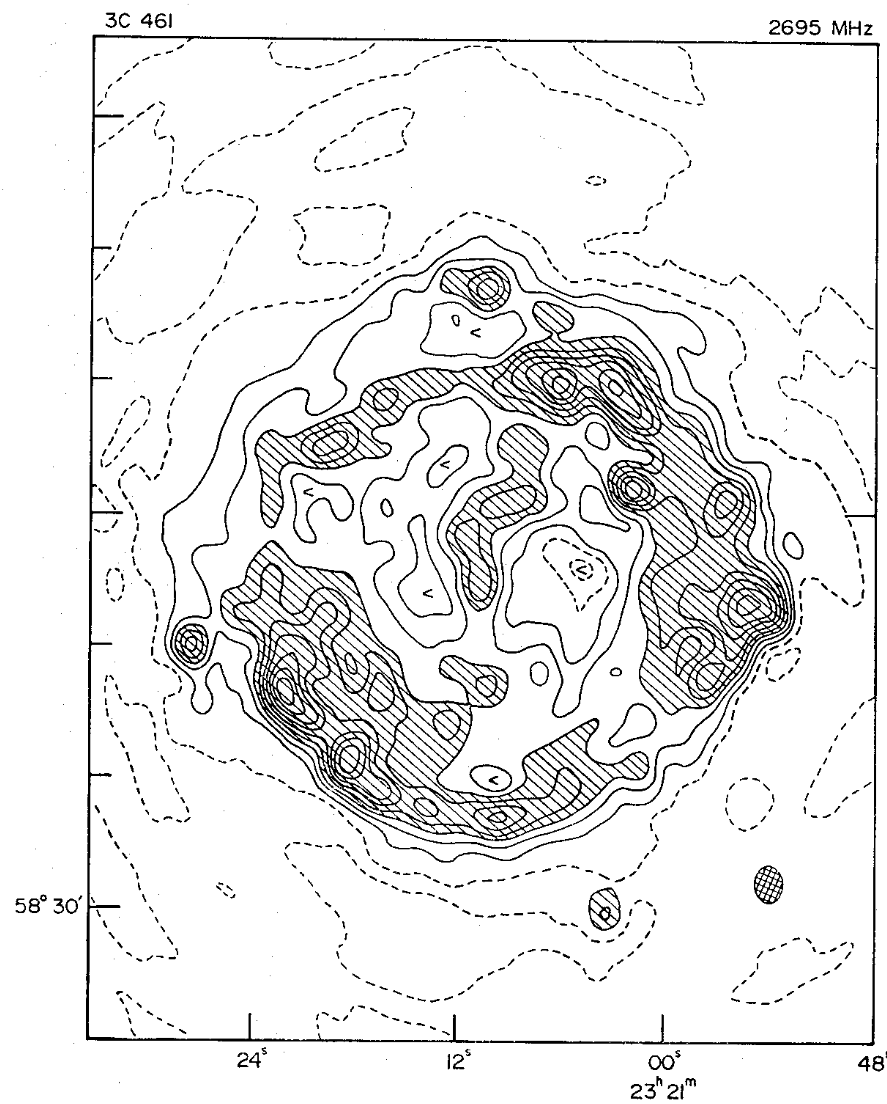


FIG. 3. *Contours of Cas A at 2·695 GHz after the correction mentioned in Section 3. The contour interval is 1100 °K. The first dashed contour represents the zero contour. The half-power beamwidth of the radio telescope (12″ × 14″ arc) is also shown.*

centre of the source. When the error is corrected, it is found that the extension of the plateau agrees on the two maps, most other details remaining unchanged. The corrected 2·7 GHz map is shown in Fig. 3.

An interesting new feature appears within the plateau, opposite the gap in the east limb of the radio shell. This broad region of enhanced emission with two local maxima is not visible on the 2·7 GHz map but, in retrospect, can be seen on the map by Ryle, Elsmore & Neville (1965) and also, more clearly, on a hitherto unpublished map at 1·4 GHz, shown in Fig. 4 (region k). This feature is coincident with one of the fast moving optical filaments discussed by Minkowski (1966) and also in Paper I; its flux density is about $2 \times 10^{-26}$ W m$^{-2}$ Hz$^{-1}$ at 5·0 GHz. The thermal emission from the optical flare, derived from the physical parameters given by Minkowski (1968), should be about $0 \cdot 2 \times 10^{-26}$ W m$^{-2}$ Hz$^{-1}$ at this frequency; the emission from this region at radio frequencies is therefore mostly non-thermal (Section 4).

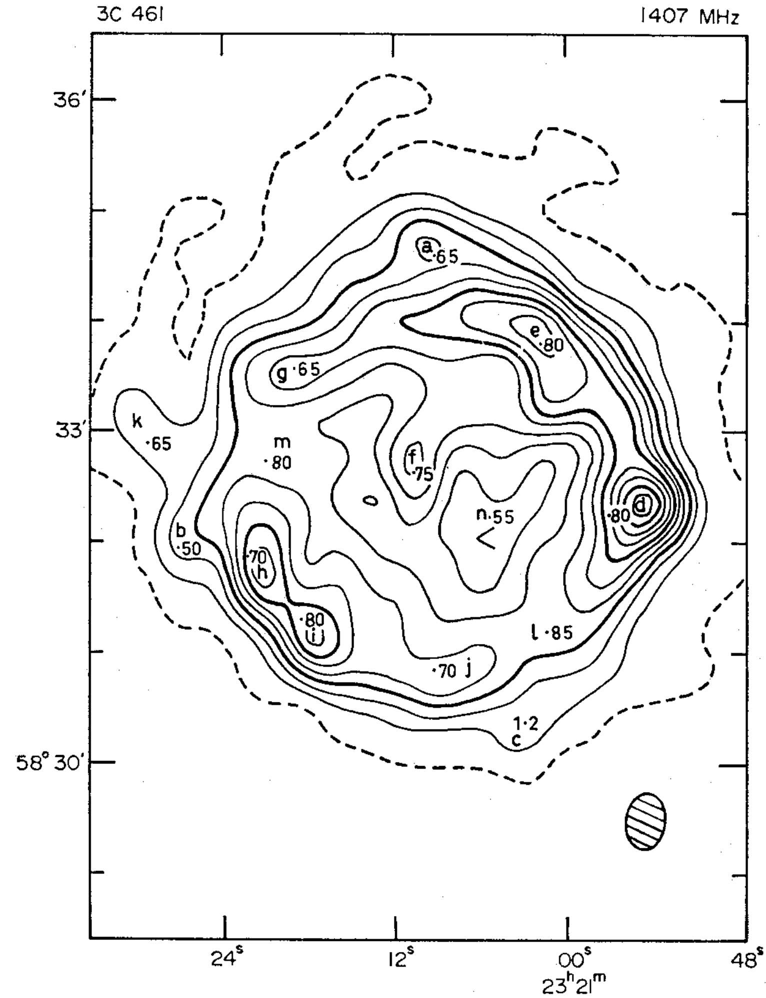


FIG. 4. *Contours of Cas A at* 1·407 *GHz, from a map taken at epoch* 1968·4. *The contour interval is* 6700 °*K. The regions studied in Section* 4 *are labelled a–n; the numbers shown represent values of spectral index for these regions. The half-power beamwidth of the radio telescope* (23″ × 27″ *arc*) *is also shown.*

## 4. CHANGES OF STRUCTURE WITH FREQUENCY

An analysis of the change of structure with frequency across the source was made in Paper I by comparing the map at 2·7 GHz presented there with the map by Ryle *et al.* (1965) at 1·4 GHz. Since the maps were made at different epochs, such an analysis also involves changes of structure with time. While the secular decrease of the total flux of Cas A is well known (Scott, Shakeshaft & Smith 1969) and can be allowed for, little is known about variations in individual features. Recent studies of the optical remnant (van den Bergh & Dodd 1970) show that the fine optical features change widely in shape in a time-scale of 10 years or less; the fine structure of the radio source might also be expected to change at a comparable rate. To test this, the 1·4 GHz map by Ryle *et al.*, made in 1965, has been compared with a more recent one made in 1968 at the same frequency (Fig. 4). Some differences in structure are found, but the errors are such that the changes cannot yet be regarded as significant.

The availability of the more recent 1·4 GHz map, that at 5·0 GHz and the corrected 2·7 GHz map, all observed within two years, now permits a more accurate study of the variations of spectral index over the source. Both the high frequency maps were convolved with smoothing functions as described in Paper I and a study of several individual regions (marked a–n in Fig. 4) was undertaken using the three maps, each with an effective resolving power of $23'' \times 27''$ arc. A power law spectrum of the form $S \propto \nu^{-\alpha}$ for constant $\alpha$ was fitted to the fluxes obtained for each region; the corresponding values of $\alpha$ are also shown in Fig. 4. The spectra of most regions are readily fitted by simple power laws, but there is the possibility of convex spectra for regions h, i and j. The scatter of the measured fluxes from the fitted lines gives errors for $\alpha$ of $\pm 0.15$ for the brighter regions and of $\pm 0.2$ or more for the weaker ones, namely a, b, c and k.

It can be seen from Fig. 4 that the values of the spectral index vary from region to region, but as a whole they are distributed about the mean value for the source ($\alpha = 0.75$) and are consistent with it within the limits of error, with the possible exceptions of the eastern extension (regions g, k and b) and of the weak central region (n). These results are in contrast with those given in Paper I, where widely different values were found for the spectral index of various regions; owing to the factors mentioned above, the present results should be taken as more reliable than the previous ones.

As a check on these results, the three maps were further convolved to an effective resolving power of $80'' \times 94''$ arc, that of a map obtained with the Cambridge One-Mile telescope at 408 MHz. This process enabled the spectra for different parts of the source enclosing the regions studied above to be extended to a lower frequency. A detailed analysis of the four maps shows that, with this resolving power, any variations of spectral index across the source are averaged, and a value of $\alpha$ near 0·75 is found for most regions, with the notable exception of the part corresponding to regions g and k above, where a value of 0·6 is found, consistent with the higher resolution results.

The 5·0 GHz map was further convolved so as to have an effective resolving power of $1'.7$ arc, comparable to that of the 19 GHz map by Mayer & Hollinger (1968), to enable a check of the above results to be extended also to a much higher frequency. Direct comparison of the brightness distributions involved uncertainties introduced by the differences in the reception patterns and sidelobe responses between the two maps; nevertheless, it appears that both the north-eastern limb of the shell and the central depression have spectral indices lower than for the rest of the source by about 0·1 to 0·2, which supports the higher resolution results.

## 5. DISTRIBUTION OF POLARIZED EMISSION

The distribution of polarized emission over the source was deduced from the three maps with feed position angles $0°$, $45°$ and $90°$, obtained as described in Section 2. The polarization response of these feed configurations in interferometers has been fully discussed by Morris, Radhakrishnan & Seielstad (1964). The circularly polarized component of the radiation was assumed to be negligible everywhere (Mayer, Hollinger & Allen 1963).

The three polarization maps were convolved with identical smoothing functions so as to obtain an effective resolving power of $23'' \times 27''$ arc; this process gave the optimum combination of signal-to-noise ratio and of resolution for the polarized intensity over the source. The convolved polarization distribution is shown in

Fig. 5. The noise level and the amount of instrumental polarization can be estimated from the magnitude and direction of the bars shown outside the source; these indicate that the polarization measured in the brighter parts of the source does not have errors greater than 2 per cent.

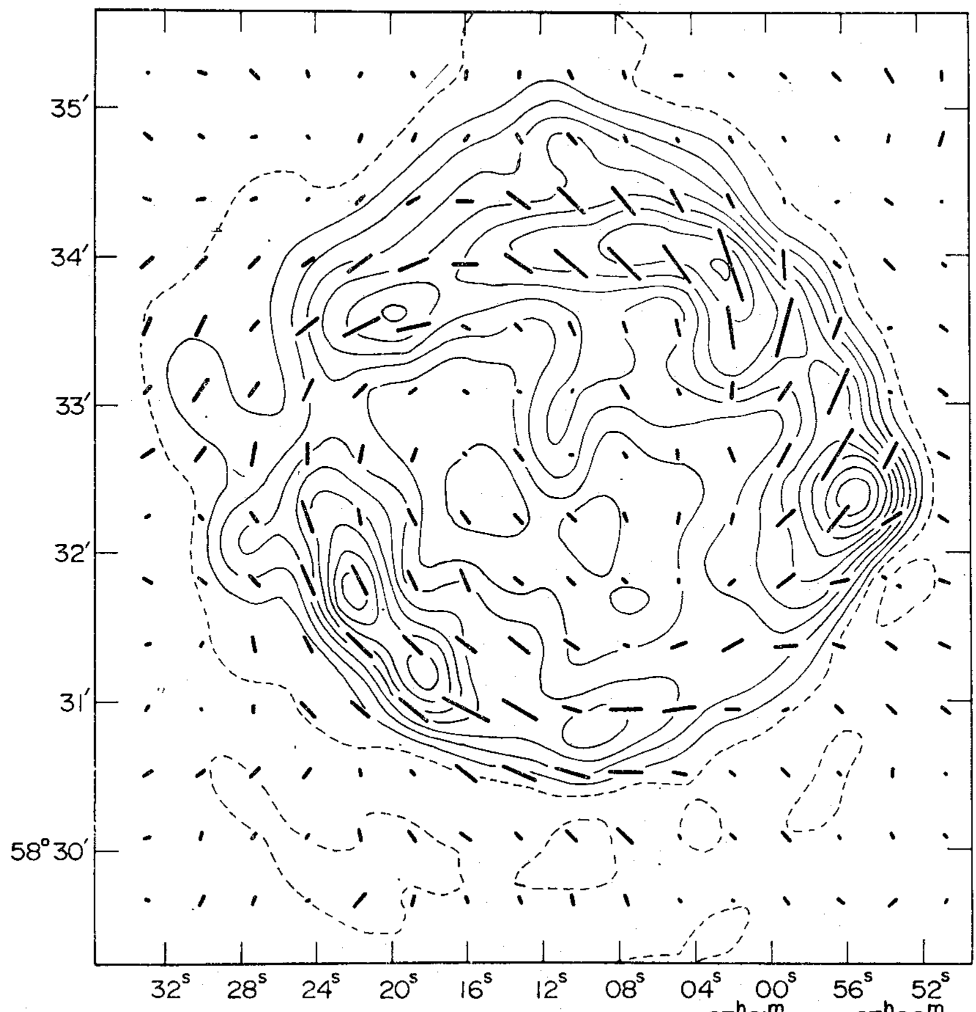


Fig. 5. *Distribution of polarized emission over Cas A at 5·0 GHz, with a resolving power of 23″ × 27″ arc, superimposed on a total intensity map at the same resolution. The bars are oriented along the position angles of the electric vectors of linear polarization and have lengths proportional to the intensity of the polarized radiation at that point. The longest bar corresponds to a brightness temperature of 100 °K at 5·0 GHz.*

The degree of polarization averages about 5 per cent around the rim of the shell, with peaks of about 10 per cent in the south-east region and of about 6 per cent in the north-west region; the central part of the shell has a degree of polarization of 1 per cent or less. The orientation of the electric vectors is approximately circumferential, in agreement with the results of Mayer & Hollinger (1968) at 19 GHz, which strongly supports the hypothesis of a radial component of magnetic field in the expanding shell of the supernova remnant.

The integrated polarization was obtained by averaging the distribution over the source and is $1 \cdot 4 \pm 0 \cdot 5$ per cent at position angle $37° \pm 15°$. The weak feature lying outside the east rim of the shell has a polarization of $9 \pm 3$ per cent, which, though only just above the noise level, is thought to be real; this result is confirmed by the recent observations of the polarization of Cas A by Baldwin *et al.* (1970) with the Cambridge Half-Mile radio telescope.

The polarization map was further convolved so as to have an effective resolving power of 1′·7 arc, comparable to that of the 19 GHz map by Mayer & Hollinger (1968), and the resulting distribution was then directly compared with that at 19 GHz. The degrees of linear polarization agree well within the uncertainties; the position angles of the electric vectors at any point differ by at most 40°, but on average a rotation of $-25° \pm 5°$ is found around the rim of the shell.

The fact that very little depolarization has occurred between 19 GHz and 5·0 GHz indicates that the Faraday rotation within the source is small at 5·0 GHz and that the rotation of position angles around the shell is due mainly to the intervening galactic medium (e.g. Gardner & Whiteoak 1963; Bologna, McLain & Sloanaker 1969). The rotation measure derived from the comparison of the two maps is about $-130$ rad m$^{-2}$ with the usual ambiguity of $n\pi$ radians in the rotation between 19 GHz and 5·0 GHz. The polarization distribution at 1·4 GHz has been observed (Seielstad & Weiler 1968, Baldwin *et al.* 1970) but the polarization is too small to give a reliable indication of position angle. The above value can, on the other hand, be compared with estimates of galactic rotation measure based on observations of polarized extra-galactic sources in the region of Cassiopeia ($l^{II} = 112°$; $b^{II} = -2°$) by Berge & Seielstad (1967); they found R.M. of $+170$ rad m$^{-2}$ for 3C 20 ($l^{II} = 122°$, $b^{II} = -11°$), of $-90$ rad m$^{-2}$ for 3C 27 ($l^{II} = 123°$, $b^{II} = 5°$), of $-400$ rad m$^{-2}$ for 3C 86 ($l^{II} = 144°$, $b^{II} = -1°$), of $-160$ rad m$^{-2}$ for 3C 430 ($l^{II} = 99°$, $b^{II} = 8°$) and of $+62$ rad m$^{-2}$ for 3C 431 ($l^{II} = 92°$, $b^{II} = 0°$). It is thus reasonable to suppose that a R.M. of $-130$ rad m$^{-2}$ is appropriate for the medium between Cas A and the Sun.

## 6. PHYSICAL CHARACTERISTICS OF THE SOURCE

The new observations at 5·0 GHz confirm satisfactorily most of the conclusions of Paper I on the physical properties of the source.

The mean profile of the map at 5·0 GHz was obtained, as described in Paper I, by averaging the emission from annuli 5″ arc wide drawn from the centre of the shell which was essentially the same as that found for the 2·7 GHz map (see Table I); the resulting mean radial profile is shown in Fig. 6.

Most of the emission from the shell can be fitted by a model distribution essentially that found in Paper I, namely a uniform, optically thin, spherical shell radiating isotropically, of outer radius $R = 130''$ arc and thickness $\Delta R = 30''$ arc. This model profile, convolved with the telescope beam, is shown superimposed on the observed profile as a smooth curve in Fig. 6. The main difference from the corresponding diagrams in Paper I is that the discrepancy between the predicted and observed emission from the centre of the shell found in the previous paper has almost completely disappeared. On closer inspection it is found that the correction made to the 2·7 GHz map (see Section 3) completely accounts for the difference, since the mean radial profile depends strongly on the large-scale components of emission. The corrected mean radial profile of the 2·7 GHz map for annuli 10″ arc wide is shown in Fig. 7 with the above model profile, convolved with the appropriate beam, superimposed.

Models of emitting shells with their magnetic field partially aligned in a radial

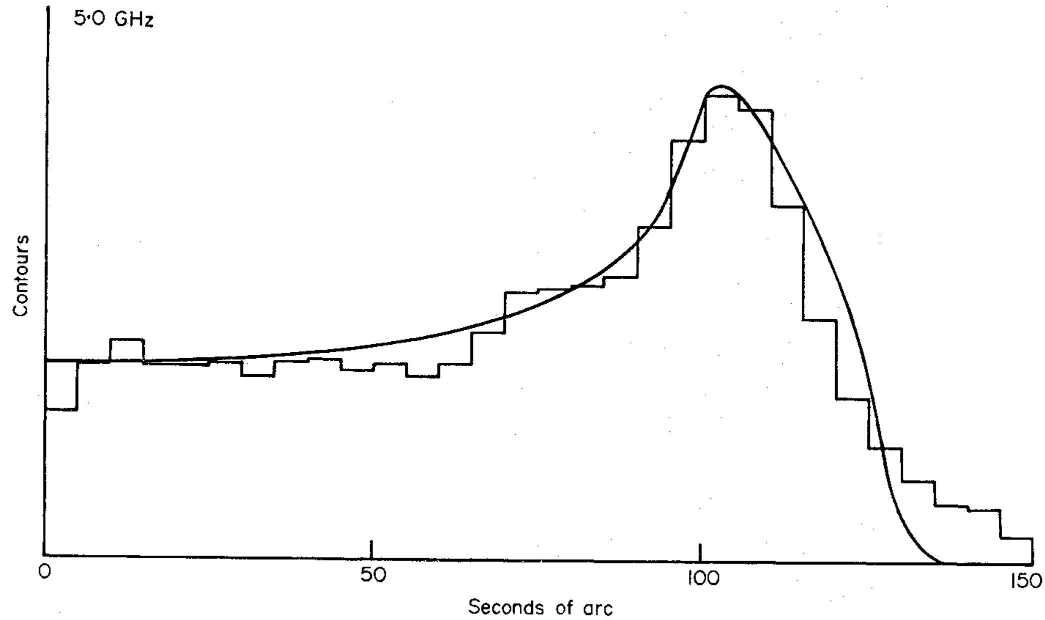


FIG. 6. *The histogram is the mean profile across Cas A at 5·0 GHz, taken at 5″ arc interval. The smooth curve corresponds to the model shell profile discussed in the text (Section 6).*

direction were also calculated as discussed in Paper I. It is found that model distributions consistent with the observed polarization described in Section 5 and requiring 6–10 per cent alignment of the field, are also consistent with the observed mean profiles of Figs 6 and 7, within the accuracy of the observations. These models thus describe satisfactorily the observed distribution at both frequencies, and the discrepancy found in Paper I, where a field alignment of 20–30 per cent was required to explain the low central emission, has been removed.

Estimates of the emitted flux and of the angular diameter of 48 out of the 80 peaks of higher emissivity mentioned in Section 3 were obtained from profiles drawn across them in two orthogonal directions; for those peaks too weak to

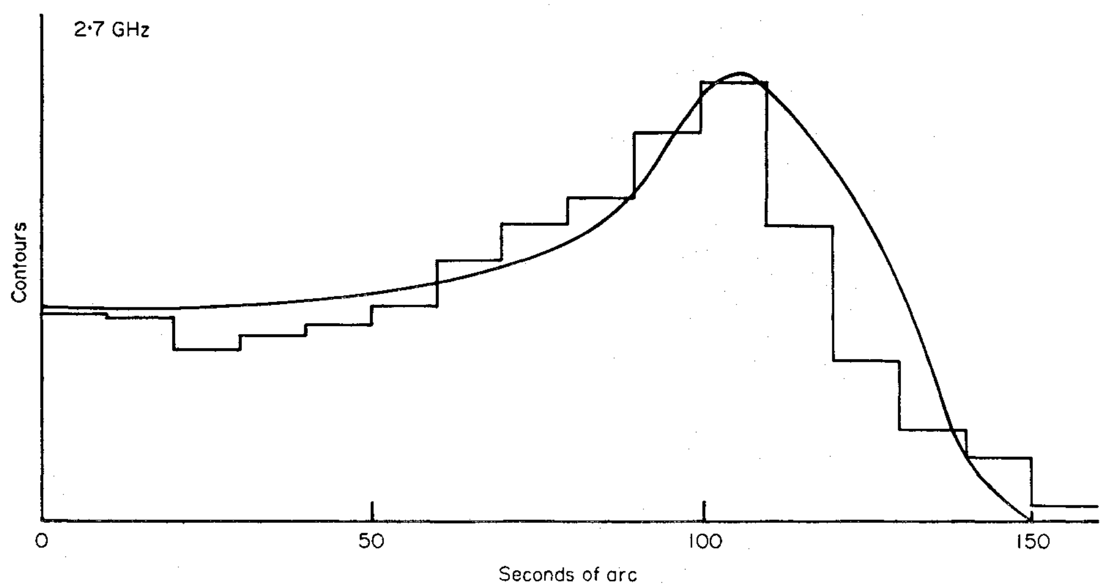


FIG. 7. *The histogram is the mean profile across Cas A at 2·7 GHz, after the correction mentioned in Section 3, taken at 10″ arc interval. The smooth curve corresponds to the model shell profile discussed in the text (Section 6).*

TABLE I

| | | (Epoch 1950·0) |
|---|---|---|
| Geometrical centre of main shell | $\alpha$ | $23^h\ 21^m\ 9^s \cdot 5$ |
| | $\delta$ | $58^\circ\ 32'\ 22''$ |
| Unweighted centre of 80 peaks | $\alpha$ | $23^h\ 21^m\ 10^s$ |
| | $\delta$ | $58^\circ\ 32'\ 29''$ |
| Weighted centre of 48 peaks | $\alpha$ | $23^h\ 21^m\ 11^s$ |
| | $\delta$ | $58^\circ\ 32'\ 42''$ |
| Weighted centre of 80 peaks | $\alpha$ | $23^h\ 21^m\ 11^s$ |
| | $\delta$ | $58^\circ\ 32'\ 39''$ |
| Optical centre of expansion* | $\alpha$ | $23^h\ 21^m\ 11^s \cdot 4$ |
| | $\delta$ | $58^\circ\ 32'\ 18'' \cdot 9$ |

* Reference: van den Bergh & Dodd (1970).

have clear enough profiles, a nominal flux of $0 \cdot 2 \times 10^{-26}$ W m$^{-2}$ Hz$^{-1}$ was assigned, corresponding to the smallest measured flux. It was thus found that the 80 regions of local maxima together contribute about 9 per cent of the total emission from the source at 5·0 GHz. Their weighted and unweighted centres of gravity were calculated and are shown in Table I; they agree reasonably well with the centre of the shell, also given in Table I.

The distribution of the 80 peaks in concentric annuli drawn at 10″ arc interval from the centre of the shell is plotted in Fig. 8. An analysis of their distribution shows that it can be fitted well by a model of discrete sources distributed uniformly within a shell of outer radius 130″ arc and thickness 30″ arc, essentially the same as for the total emission, together with a low density tail beyond this shell. The model distribution, normalized to the same number of objects, is also shown in Fig. 8. This model distribution differs from that found in Paper I for the 25

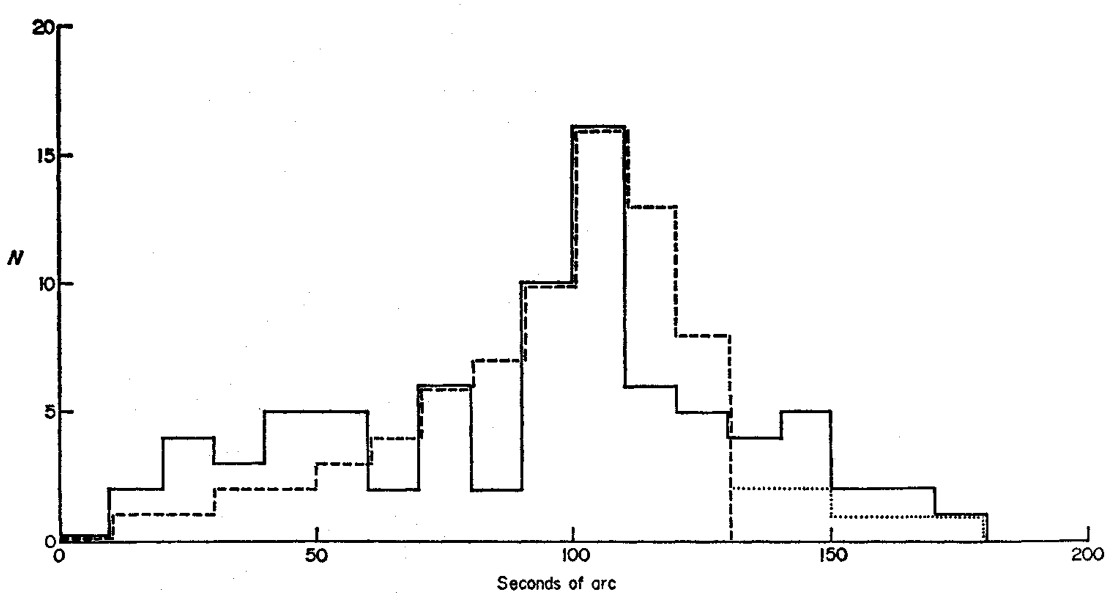


FIG. 8. *The continuous histogram is the observed distribution of* 80 *local emission maxima over Cas A. The dashed histogram corresponds to the model distribution within the shell discussed in the text and the dotted one is a low density tail* (*Section* 6).

TABLE II

| Quantity | Average (and r.m.s. deviation) for 48 peaks | Main shell |
|---|---|---|
| Flux density at 5·0 GHz ($S_5$) ($10^{-26}$ W m$^{-2}$ Hz$^{-1}$) | 1·6 (±1·3) | 900±30 |
| Angular size ($\theta$) (″ arc) | 7·7 (±3·2) | $R$ = 130±5<br>$\Delta R$ = 30±5 |
| Physical size ($L$) (pc) | 0·13 (±0·05) | $R$ = 2·1<br>$\Delta R$ = 0·6 |
| Minimum total ($U_{min}$) electron energy (erg) | $3·5\ (\pm 3·1) \times 10^{45}$ | $\sim 10^{49}$ |
| Magnetic field $B$ for equipartition (Gauss) | $1·2\ (\pm 0·4) \times 10^{-3}$ | $\sim 5 \times 10^{-4}$ |
| Emissivity relative to main shell | 120 (±180) | 1 |

regions of enhanced emission discussed there, which were fitted better by a thin shell rather than by a thick one. Owing to the higher resolving power, however, many local emission maxima appear on the 5·0 GHz map in regions which were not considered peaks on the 2·7 GHz map; the two results do not, therefore, contradict each other.

Those local emission maxima arising from further resolution of the above 25 peaks do not account, in general, for more than a fraction of the flux from the corresponding regions at 2·7 GHz (Fig. 3); the same can be said of the latter when compared with the enhanced emission regions on the 1·4 GHz map (Fig. 4), assuming in both cases an average spectral index of 0·75 (Section 4). This consideration suggests that, although with each increase in resolving power even finer features are revealed within the emission regions, they are superimposed on the larger structure and do not break it down completely; the fluxes and angular sizes derived above are in this case significant for the structure seen at 5·0 GHz. Estimates of some physical quantities for the 48 peaks of known flux and angular size were calculated using the expressions for the minimum total energy from synchrotron radiation by relativistic electrons only, given by Ginzburg & Syrovatskii (1965); the lowest frequency at which the regions have a simple power law spectrum was assumed to be 10 MHz. The average values of these quantities and their r.m.s. deviations are given in Table II, with the corresponding values for the shell as a whole given for comparison. The values of these quantities for the three separated regions discussed in detail in Paper I (in the case of the northern

TABLE III

| Quantity | I* | II* | III* |
|---|---|---|---|
| Flux density at 5·0 GHz ($S_5$) ($10^{-26}$ W m$^{-2}$ Hz$^{-1}$) | 2·7 | 3·2 | 1·2 |
| Angular size ($\theta$) (″ arc) | 9·0 | 7·6 | 5·8 |
| Physical size ($L$) (pc) | 0·15 | 0·13 | 0·10 |
| Minimum total ($U_{min}$) electron energy (erg) | $5·0\ 10^{45}$ | $4·4\ 10^{45}$ | $1·8\ 10^{45}$ |
| Magnetic field $B$ for equipartition (Gauss) | $1·1\ 10^{-3}$ | $1·4\ 10^{-3}$ | $1·3\ 10^{-3}$ |
| Emissivity relative to main shell | 63 | 120 | 110 |

* I North of shell (see Paper I).
II East of shell (see Paper I).
III South of shell (see Paper I).

region, which has been split into several maxima, for the main component) are given separately in Table III; it can be seen that the estimates of their angular sizes agree with the upper limits found in Paper I.

## 7. SUMMARY OF RESULTS

(a) Cassiopeia A is about 5 per cent linearly polarized at 5·0 GHz; the polarization distribution agrees with that found by Mayer & Hollinger (1968) at 19 GHz if a rotation measure of about $-130$ rad $m^{-2}$ is adopted. This polarization indicates a slight preferential alignment of the magnetic field in a radial direction.

(b) The mean radial distribution of the emission from the source is consistent with a uniformly radiating shell of outer radius 130″ arc and thickness 30″ arc in which the magnetic field is preferentially aligned in a radial direction to the extent shown by the polarization observations.

(c) About 9 per cent of the radiation comes from peaks of emission the angular sizes of which are comparable with the beamwidth ($6''\cdot5 \times 7''\cdot6$ arc). The spatial distribution of these peaks is also consistent with a uniform distribution in a shell of outer radius 130″ arc and thickness 30″ arc.

(d) The main shell is surrounded by a further plateau of relatively weak emission around most of its circumference; this region also contains several small intense peaks of emission. One of the latter coincides in position with one of the fast optical filaments at position angle 70° from the centre of the shell (Minkowski 1966).

(e) The spectral index over most of the source is 0·75 to within the limits of error, except for two regions which show a somewhat flatter spectrum.

## ACKNOWLEDGMENTS

The author is indebted to Mr C. A. Murray of the Royal Greenwich Observatory for accurate positions of stars in the field of Cassiopeia A, to Professor S. van den Bergh for the use of his 200-inch photograph and to Drs C. H. Mayer and J. P. Hollinger for detailed information on their observations. He also thanks all the members of the Department for their help and encouragement, in particular Drs P. A. G. Scheuer and J. R. Shakeshaft. The receipt of a University Research Maintenance Fund grant is also gratefully acknowledged.

*Mullard Radio Astronomy Observatory, Cavendish Laboratory, Cambridge*

## REFERENCES

Baldwin, J. E., Jennings, J. E., Shakeshaft, J. R., Warner, P. J., Wilson, D. M. A. & Wright, M. C. H., 1970. *Mon. Not. R. astr. Soc.*, (submitted).
Berge, G. L. & Seielstad, G. A., 1967. *Astrophys. J.*, **148**, 367.
Bergh, S. van den & Dodd, W. W., 1970. Preprint.
Bologna, J. M., McLain, E. F. & Sloanaker, R. M., 1969. *Astrophys. J.*, **156**, 815.
Elsmore, B., Kenderdine, S. & Ryle, M., 1966. *Mon. Not. R. astr. Soc.*, **134**, 87.
Gardner, F. F. & Whiteoak, J. B., 1963. *Nature, Lond.*, **197**, 1162.
Ginzburg, V. L. & Syrovatskii, S. I., 1965. *A. Rev. Astr. Astrophys.*, **3**, 297.
Hogg, D. E., Macdonald, G. H., Conway, R. G. & Wade, C. M., 1969. *Astr. J.*, **74**, 1206.
Kellermann, K. I., Pauliny-Toth, I. I. K. & Williams, P. J. S. 1969. *Astrophys. J.*, **157**, 1.

Mayer, C. H. & Hollinger, J. P., 1968. *Astrophys. J.*, **151**, 53.
Mayer, C. H., Hollinger, J. P. & Allen, P. J., 1963. *Astrophys. J.*, **137**, 1309.
Minkowski, R., 1966. *Nature, Lond.*, **209**, 1339.
Minkowski, R., 1968. *Nebulae and Interstellar Gas*, Ch. 11, eds B. Middlehurst & L. Aller, University of Chicago Press.
Morris, D., Radhakrishnan, V. & Seielstad, G. A., 1964. *Astrophys. J.*, **139**, 551.
Rosenberg, I., 1970. *Mon. Not. R. astr. Soc.*, **147**, 215.
Ryle, M., 1962. *Nature, Lond.*, **194**, 517.
Ryle, M., Elsmore, B. & Neville, A. C., 1965. *Nature, Lond.*, **205**, 1259.
Seielstad, G. A. & Weiler, K. W., 1968. *Astrophys. J.*, **154**, 817.
Sastry, C. V., Pauliny-Toth, I. I. K. & Kellermann, K. I., 1967. *Astr. J.*, **72**, 230.
Scott, P. F., Shakeshaft, J. R. & Smith, M. A., 1969. *Nature, Lond.*, **223**, 1139.